JACS
JOURNAL OF THE AMERICAN CHEMICAL SOCIETY
Communication
pubs.acs.org/JACS

Controlled Synthesis of Topological Insulator Nanoplate Arrays on Mica

Hui Li,[†,§] Jie Cao,[†,§] Wenshan Zheng,[†,§] Yulin Chen,[‡,§] Di Wu,[†] Wenhui Dang,[†] Kai Wang,[†] Hailin Peng,*[,†] and Zhongfan Liu*[,†]

[†]Center for Nanochemistry, Beijing National Laboratory for Molecular Sciences (BNLMS), State Key Laboratory for Structural Chemistry of Unstable and Stable Species, College of Chemistry and Molecular Engineering, Peking University, Beijing 100871, P. R. China

[‡]Department of Physics and Clarendon Laboratory, University of Oxford, Parks Road, Oxford OX1 3PU, U.K.

Supporting Information

ABSTRACT: The orientation- and position-controlled synthesis of single-crystal topological insulator (Bi_2Se_3 and Bi_2Te_3) nanoplate arrays on mica substrates was achieved using van der Waals epitaxy. Individual ultrathin nanoplates with the lateral dimension up to ~0.1 mm or uniform thickness down to 1−2 nm were produced. Single-Dirac-cone surface states of nanoplate aggregates were confirmed by angle-resolved photoemission spectroscopy measurements. The large-grain-size, single-crystal nanoplate arrays grown on mica can act as facile platforms for a combination of spectroscopy and in situ transport measurements, which may open up new avenues for studying exotic physical phenomena, surface chemical reactions, and modification in topological insulators.

Quasi-two-dimensional (quasi-2D) atomic crystals can be considered as individual atomic planes isolated from a large variety of strongly layered materials such as graphite, hexagonal boron nitride, transition-metal oxides, metal chalcogenides, and metal iodides.[1] The unique physical and chemical properties of quasi-2D crystals have made a profound impact on fundamental research and technological applications in electronics, spintronics, photonics, catalytic chemistry, and energy science.[2] Recently, the layered V−VI binary compounds Bi_2Se_3, Bi_2Te_3, and Sb_2Te_3 and their ternary compounds were discovered as three-dimensional topological insulators, a new state of quantum matter with an insulating bulk gap and massless Dirac surface states topologically protected with helical spin texture.[3−5] Since their discovery, topological insulators have brought great opportunities and challenges to chemists and materials scientists. In particular, the ultralow-dissipation surface states of topological insulators are inherently robust in comparison with conventional surface states, thus paving the way toward novel electronics, optoelectronics, energy conversion, and catalytic chemistry.[6−8]

Few-layer topological insulator nanoribbons, nanoplates, or nanosheets have very large surface-to-volume ratios that can significantly enhance the contribution of exotic surface states, and their unique quasi-2D geometry also facilitates their integration into functional devices for manipulation and manufacturing.[6,9−16] Motivated by these advantages, we explored the vapor−liquid−solid growth of nanoribbons and the catalyst-free vapor−solid growth of nanoplates on oxidized silicon substrates and graphene, respectively.[9,17−19] Weak antilocalization behavior, the ambipolar field effect, the Aharonov−Bohm (AB) effect, and Shubnikov−de Haas (SdH) oscillation have recently been observed in such topological insulator quasi-2D nanostructures.[9,18,20−24] However, to realize fully the technological potential of high-quality topological insulator quasi-2D nanostructures, controllable synthesis is an essential and challenging task that requires accurate control of the orientation, thickness, position, and layout.

Here we demonstrate a facile, high-yield method for growing single-crystal nanoplate arrays of Bi_2Se_3 and Bi_2Te_3 with well-aligned orientation, controlled thickness, and specific placement on mica substrates by van der Waals epitaxy. Well-defined nanoplate arrays of Bi_2Se_3 and Bi_2Te_3 were formed by selective nucleation and growth at desired locations on a patterned mica surface. Single-crystalline nanoplates with uniform thickness and large lateral dimensions were produced. Furthermore, the high-quality, large-area nanoplates grown on transparent insulating mica substrates can serve as a straightforward platform for spectroscopy, device fabrication, and electronic measurements. The single-Dirac-cone surface state nature of nanoplate aggregates was confirmed by angle-resolved photoemission spectroscopy (ARPES). Also, the combination of vibrational spectroscopy with electrical transport measurements may be an effective approach for studying the structural correlation with physical properties of individual topological insulator nanoplates.

Van der Waals epitaxy is a powerful technique for the growth of high-crystalline-quality nanostructures from various compounds onto a substrate without surface dangling bonds, regardless of their lattice mismatch. In particular, nanowire arrays, tripodal nanostructures, and quasi-2D layered structures with van der Waals gaps were successfully synthesized using this universal epitaxy.[17,25−29] The layered topological insulator Bi_2X_3 (X = Se, Te) has a rhombohedral crystal structure in the space group D_{3d}^5 ($R\bar{3}m$).[30] Each planar quintuple layer (QL) with a thickness of ~1 nm consists of covalently bonded X−Bi−X−Bi−X sheets (Figure 1A). The QLs are held together by

Received: March 4, 2012
Published: March 28, 2012

dx.doi.org/10.1021/ja3021395 | J. Am. Chem. Soc. 2012, 134, 6132−6135

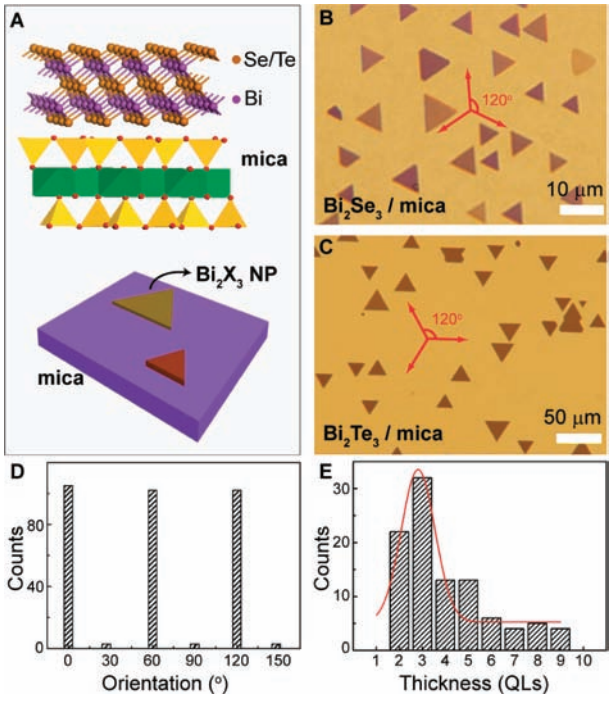

Figure 1. (A) Schematic of nanoplates (NPs) of Bi_2Se_3 and Bi_2Te_3 epitaxially grown on a synthesized mica substrate via van der Waals epitaxy. (B, C) Typical transmission-mode OM images of NP arrays of Bi_2Se_3 and Bi_2Te_3 on transparent mica substrates, respectively. (D) Histogram of the orientation distribution of triangular Bi_2Te_3 nanoplates obtained from a substrate area of ~300 μm × 300 μm. (E) Thickness distribution histogram for Bi_2Se_3 triangular NPs obtained from substrate area of ~500 μm × 500 μm.

van der Waals interactions. Fluorophlogopite mica [$KMg_3(AlSi_3O_{10})F_2$], an ideal substrate for van der Waals epitaxy of Bi_2X_3, has a layered structure with pseudohexagonal Z_2O_5 layers (Z = Si, Al).[11] Because of the relatively weak interlayer bonds, the atomically smooth surface of fluorophlogopite mica can be readily and repeatedly renewed by perfect cleavage parallel to the (001) plane. This chemically inert substrate can relax stringent lattice matching conditions, facilitating the epitaxial growth of large-area, high-quality nanoplates of Bi_2Se_3 and Bi_2Te_3 in a setup similar to our previous nanoribbon and nanoplate synthesis (see Figure S1 in the Supporting Information for experimental details).[9,18]

As-obtained nanoplates of Bi_2Se_3 and Bi_2Te_3 on transparent mica substrates were first identified by their contrast in transmission-mode optical microscopy (OM) images. As shown in Figure 1B,C, triangular semitransparent Bi_2Se_3 and Bi_2Te_3 nanoplates with thickness-dependent optical contrast and identical orientations were clearly seen. The lateral dimension of the nanoplates ranged from several to hundreds of micrometers. In contrast to the random orientation of the nanoplates grown on SiO_2/Si substrates,[18] the nanoplates' edges on mica were oriented predominantly at multiples of ~60° (Figure 1D), consistent with the 2D triangular lattice of the Bi_2X_3 QL. The observation of orientation-controlled nanoplate alignment suggests the epitaxial nature of Bi_2X_3 nanoplates on mica. Scanning electron microscopy (SEM) images also confirmed that few-layer Bi_2X_3 nanoplates were aligned in the same orientation on the mica surface (Figure S2). Remarkably, most of the individual nanoplates had uniform thickness along the entire plane. The thickness distribution of nanoplates was found to be relatively sharp. For example, Bi_2Se_3 nanoplates obtained in a substrate area of 500 μm × 500 μm exhibited a thickness distribution of 2−9 QLs in the OM images (Figure 1E). Notably, ultrathin nanoplates of Bi_2Se_3 and Bi_2Te_3 with thickness of 1 QL were nearly invisible in the OM images because of their light contrast. However, 1 QL thick nanoplates grown on mica were clearly identified using atomic force microscopy (AFM) (Figure S3), which has not been achieved on the SiO_2 substrate.[18]

These ultrathin nanoplates are single-crystalline rhombohedral phase with flat surfaces and atomically smooth edges parallel to the $(11\bar{2}0)$ direction, as shown by transmission electron microscopy (TEM) and selected-area electron diffraction (SAED) (Figure S4). A folded edge of a Bi_2Te_3 nanoplate exhibits a layered structure with alternating bright and dark fringes, corresponding to steps between adjacent QLs (Figure S4). Energy-dispersive X-ray spectroscopy (EDX) analyses revealed uniform chemical composition along the entire plane with a Bi/X atomic ratio of 2:3 (Figure S5). Micro-Raman spectroscopy and 2D Raman mapping were also conducted to confirm the structural and compositional uniformity of the nanoplates (Figure S6).

In addition to the orientation and thickness control during growth, precise control of the positions of the single-crystalline nanoplate arrays will be crucial in the subsequent integration of these nanostructures. Bi_2X_3 nanoplates usually nucleated from random locations on a perfectly flat surface of mica. However, once the initial nucleation was positioned at specific locations, the subsequent growth of nanoplates was locally confined (Figure S7), leading to the formation of nanoplate arrays of single crystals. For this purpose, we used selective oxygen plasma etching to modify specific regions of the mica surface, with patterned PMMA films or copper grids as lithography masks. In the etched regions of the mica surface, dramatic changes in the topography and chemical composition could occur,[31] thus hindering the van der Waals epitaxy of single-crystal Bi_2X_3 nanoplates. In contrast, the unetched regions of mica surface enabled the deposition of Bi_2X_3 nanoplates by means of van der Waals epitaxy in a given experiment. Figure 2A,B shows ordered arrays of round and triangular Bi_2Se_3 nanoplates, respectively, with thicknesses of 3−8 nm on mica substrates with predesigned patterns. A well-ordered 11 × 14 array of truncated triangular Bi_2Te_3 nanoplates was also created on the mica surface (Figure 2C). An AFM image and height profile (corresponding to the white line in the image) of a ~20 QL thick Bi_2Te_3 nanoplate is shown in Figure 2D. From the optical and AFM images of nanoplate arrays, most of the single-crystal nanoplates have flat surfaces, which is reminiscent of a layer-by-layer growth mechanism.[32]

Large-area, high-crystalline-quality nanoplates of topological insulators grown on transparent insulating mica substrates can provide a facile platform for spectroscopic characterization, device fabrication, and electronic measurements. It will clearly be necessary to prepare large-grain-size, single-crystal nanoplates without dislocations and grain boundaries. In principle, suppressing the nucleation density and reducing the vapor source is a feasible approach for the growth of large-size single-crystal domains. We achieved the growth of single-crystal Bi_2Te_3 nanoplates with domains of up to 0.1 mm in size using a very low vapor pressure process. For example, Figure 3A shows a typical optical image of an individual Bi_2Te_3 nanoplate with lateral dimensions exceeding 0.1 mm epitaxially grown on mica. The corresponding AFM image and height profile of the Bi_2Te_3

dx.doi.org/10.1021/ja3021395 | J. Am. Chem. Soc. 2012, 134, 6132−6135

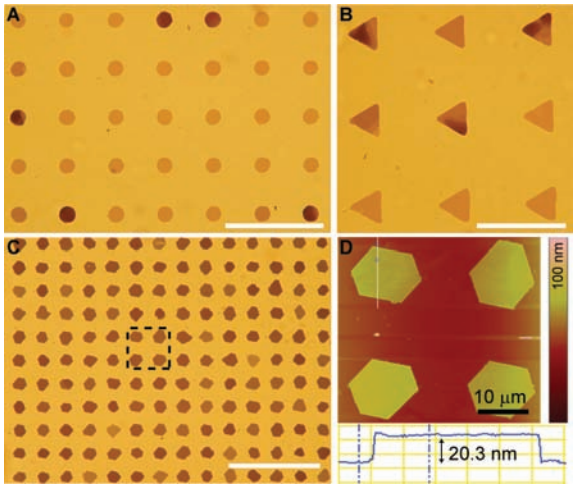

Figure 2. (A, B) OM images of 5 × 7 and 3 × 3 arrays of round and triangular Bi_2Se_3 nanoplates, respectively, on mica. (C) OM image of 11 × 14 Bi_2Te_3 nanoplate array on mica. (D) AFM image of the 2 × 2 Bi_2Te_3 nanoplate array shown in the dashed black box in (C) and the corresponding height profile along the white line in the AFM image. Scale bars in (A–C), 100 μm.

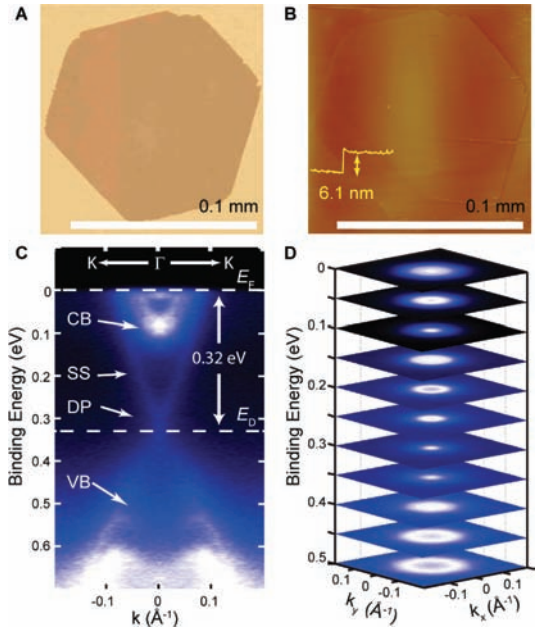

Figure 3. (A) OM image and (B) corresponding AFM image and height profile of a large-size, single-crystal Bi_2Te_3 nanoplate with a thickness of 6 QLs grown on mica. (C) Electronic band dispersion along the K–Γ–K direction of large-scale Bi_2Se_3 nanoplate aggregates grown on a mica substrate as measured by ARPES. A direct band gap between the conduction band (CB) and valence band (VB) and a Dirac-cone-type surface state (SS) were identified. (D) Constant-energy contour images of the band structure as functions of k_x and k_y at particular binding energies.

nanoplate reveal a very flat surface with a uniform thickness of 6 QLs (Figure 3B).

As the growth continues, oriented nanoplate arrays grown up from different nuclei can eventually coalesce to form large-size nanoplate aggregates on mica (Figure S7). It is relatively easy to characterize the electronic band structures of the large-area-domain nanoplate aggregates using ARPES measurements. As shown in Figure 3C, the ARPES data for Bi_2Se_3 nanoplate aggregates unambiguously revealed a direct bulk gap and surface states consisting of a single Dirac cone, characteristic of the topological insulator.[3,4] 2D contour plots of the Dirac-like dispersion at various binding energies are shown in Figure 3D. Although the bulk conduction band (CB) is partially occupied, indicative of n-type doping, the Dirac surface state band is clearly visible, exhibiting the X-shaped linear dispersion with its Dirac point (DP) at ~0.32 eV below the Fermi level (E_F). These observations confirm the high crystalline quality and robust topological surface states of nanoplate aggregates.

For the device fabrication and electronic measurements, a six-terminal Hall-bar electrode was directly patterned on an individual nanoplate by conventional photolithography (the nanoplate was large enough to be visible in OM during the photolithographic process; see Figure 4A). Ohmic contacts to

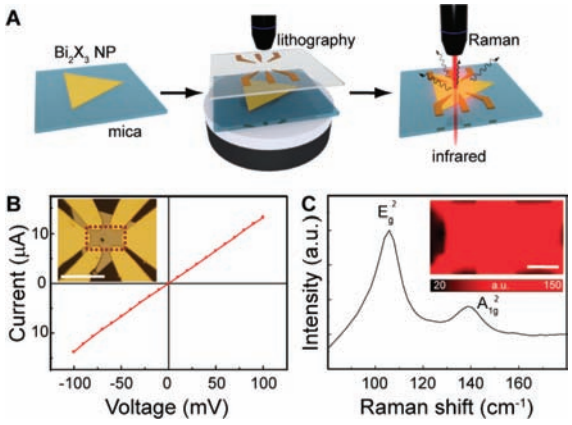

Figure 4. (A) Schematic of the photolithographic fabrication process and Raman and micro-infrared spectroscopy characterizations of large-size single-crystal nanoplates on a mica substrate. (B) Typical I–V curve of a Bi_2Te_3 nanoplate. Inset: optical image of a fabricated device used for the electric measurement. Scale bar, 50 μm. (C) Raman measurement of the same Bi_2Te_3 nanoplate. Inset: E_g^2 band Raman map of the selected region indicated by the dashed red box in the inset of (B). Scale bar, 10 μm.

the nanoplate were deposited by thermal evaporation of Cr/Au (5 nm/50 nm). Four-point probe measurements were conducted to remove the effect of contact resistance. As shown in Figure 4B, the source-drain current (I) versus voltage (V) characteristic of an individual Bi_2Te_3 nanoplate is linear and symmetric, with a four-probe resistance of 7.4 kΩ.

Together with transport measurements, vibrational spectroscopic techniques such as Raman and IR absorption spectroscopy are noninvasive probes for the chemical fingerprint and structural information of topological insulator nanoplates. As a proof of concept, we demonstrated both micro-Raman and micro-IR spectroscopy measurements on an individually fabricated Bi_2Te_3 nanoplate device (Figure 4 and Figure S8). The micro-Raman spectrum of a selected region of a Bi_2Te_3 nanoplate device was collected to qualify further the structure of nanoplates with a spatial resolution in the range of 1 μm. As shown in the Figure 4C inset, the micro-Raman map of the intensity of the Bi_2Te_3 E_g^2 band has a uniformly distributed color. This observation indicates the high homogeneity of the Bi_2Te_3 nanoplate, consistent with the uniform thickness of the nanoplate observed with AFM and TEM.

In summary, ultrathin, single-crystal topological insulator nanoplate arrays with aligned orientation and specific place-

dx.doi.org/10.1021/ja3021395 | J. Am. Chem. Soc. 2012, 134, 6132–6135

ments were successfully synthesized on mica substrates using van der Waals epitaxy. The control over the nucleation site on a mica surface allowed us to grow high-yield, well-defined nanoplate arrays. Single-crystalline nanoplates with a uniform thickness down to 1−2 nm were obtained. The lateral dimensions of ultrathin nanoplates can be up to 0.1 mm. Single-Dirac-cone surface states of nanoplate aggregates were identified by ARPES measurements. The large-gain-size, single-crystal nanoplate array can act as an ideal platform for spectroscopic characterization, device fabrication, and electronic measurements. The combination of vibrational spectroscopy and in situ transport measurements on individual single crystal nanoplates may pave the way for studying phonons, electrons, electron−phonon interactions, and surface chemistry in topological insulators.

■ ASSOCIATED CONTENT

Supporting Information

Experimental details and supporting figures. This material is available free of charge via the Internet at http://pubs.acs.org.

■ AUTHOR INFORMATION

Corresponding Author

hlpeng@pku.edu.cn; zfliu@pku.edu.cn

Author Contributions

[§]These authors contributed equally.

Notes

The authors declare no competing financial interest.

■ ACKNOWLEDGMENTS

We thank Alan Y. Liu for helpful discussions and acknowledge financial support by the National Science Foundation of China (20973007, 51121091, 21173004, 11104003) and the National Basic Research Program of China (2012CB933404, 2011CB921904, 2011CB933003), NCET, and SRF for ROCS and SEM; Y.C. acknowledges support from a U.S. DARPA MESO Project (N66001-11-1-4105).

■ REFERENCES

(1) Novoselov, K. S.; Jiang, D.; Schedin, F.; Booth, T. J.; Khotkevich, V. V.; Morozov, S. V.; Geim, A. K. *Proc. Natl. Acad. Sci. U.S.A.* **2005**, *102*, 10451.

(2) Geim, A. K. *Science* **2009**, *324*, 1530.

(3) Zhang, H.; Liu, C.-X.; Qi, X.-L.; Dai, X.; Fang, Z.; Zhang, S.-C. *Nat. Phys.* **2009**, *5*, 438.

(4) Xia, Y.; Qian, D.; Hsieh, D.; Wray, L.; Pal, A.; Lin, H.; Bansil, A.; Grauer, D.; Hor, Y. S.; Cava, R. J.; Hasan, M. Z. *Nat. Phys.* **2009**, *5*, 398.

(5) Chen, Y. L.; Analytis, J. G.; Chu, J. H.; Liu, Z. K.; Mo, S.-K.; Qi, X. L.; Zhang, H. J.; Lu, D. H.; Dai, X.; Fang, Z.; Zhang, S. C.; Fisher, I. R.; Hussain, Z.; Shen, Z.-X. *Science* **2009**, *325*, 178.

(6) Kong, D.; Cui, Y. *Nat. Chem.* **2011**, *3*, 845.

(7) Qi, X.-L.; Zhang, S.-C. *Rev. Mod. Phys.* **2011**, *83*, 1057.

(8) Hasan, M. Z.; Kane, C. L. *Rev. Mod. Phys.* **2010**, *82*, 3045.

(9) Peng, H. L.; Lai, K.; Kong, D.; Meister, S.; Chen, Y.; Qi, X.-L.; Zhang, S.-C.; Shen, Z.-X.; Cui, Y. *Nat. Mater.* **2010**, *9*, 225.

(10) Li, H.; Peng, H. L.; Dang, W.; Yu, L.; Liu, Z. F. *Front. Phys.* **2012**, *7*, 208.

(11) Peng, H. L.; Dang, W.; Cao, J.; Chen, Y.; Wu, D.; Zheng, W.; Li, H.; Shen, Z.-X.; Liu, Z. F. *Nat. Chem.* **2012**, *4*, 281.

(12) Cho, S.; Kim, D.; Syers, P.; Butch, N. P.; Paglione, J.; Fuhrer, M. S. *Nano Lett.* **2012**, *12*, 469.

(13) Min, Y.; Moon, G. D.; Kim, B. S.; Lim, B.; Kim, J.-S.; Kang, C. Y.; Jeong, U. *J. Am. Chem. Soc.* **2012**, *134*, 2872.

(14) Zhang, J.; Peng, Z.; Soni, A.; Zhao, Y.; Xiong, Y.; Peng, B.; Wang, J.; Dresselhaus, M. S.; Xiong, Q. *Nano Lett.* **2011**, *11*, 2407.

(15) Teweldebrhan, D.; Goyal, V.; Balandin, A. A. *Nano Lett.* **2010**, *10*, 1209.

(16) Teweldebrhan, D.; Goyal, V.; Rahman, M.; Balandin, A. A. *Appl. Phys. Lett.* **2010**, *96*, No. 053107.

(17) Dang, W.; Peng, H. L.; Li, H.; Wang, P.; Liu, Z. F. *Nano Lett.* **2010**, *10*, 2870.

(18) Kong, D.; Dang, W.; Cha, J. J.; Li, H.; Meister, S.; Peng, H. L.; Liu, Z. F.; Cui, Y. *Nano Lett.* **2010**, *10*, 2245.

(19) Kong, D. S.; Randel, J. C.; Peng, H. L.; Cha, J. J.; Meister, S.; Lai, K. J.; Chen, Y. L.; Shen, Z. X.; Manoharan, H. C.; Cui, Y. *Nano Lett.* **2010**, *10*, 329.

(20) Xiu, F.; He, L.; Wang, Y.; Cheng, L.; Chang, L.-T.; Lang, M.; Huang, G.; Kou, X.; Zhou, Y.; Jiang, X.; Chen, Z.; Zou, J.; Shailos, A.; Wang, K. L. *Nat. Nanotechnol.* **2011**, *6*, 216.

(21) Chen, J.; Qin, H. J.; Yang, F.; Liu, J.; Guan, T.; Qu, F. M.; Zhang, G. H.; Shi, J. R.; Xie, X. C.; Yang, C. L.; Wu, K. H.; Li, Y. Q.; Lu, L. *Phys. Rev. Lett.* **2010**, *105*, No. 176602.

(22) Steinberg, H.; Gardner, D. R.; Lee, Y. S.; Jarillo-Herrero, P. *Nano Lett.* **2010**, *10*, 5032.

(23) Granqvist, C. G. *Sol. Energy Mater. Sol. Cells* **2007**, *91*, 1529.

(24) Kong, D.; Chen, Y.; Cha, J. J.; Zhang, Q.; Analytis, J. G.; Lai, K.; Liu, Z.; Hong, S. S.; Koski, K. J.; Mo, S.-K.; Hussain, Z.; Fisher, I. R.; Shen, Z.-X.; Cui, Y. *Nat. Nanotechnol.* **2011**, *6*, 705.

(25) Koma, A. *Thin Solid Films* **1992**, *216*, 72.

(26) Koma, A. *J. Cryst. Growth* **1999**, *201*, 236.

(27) Yan, K.; Peng, H. L.; Zhou, Y.; Li, H.; Liu, Z. F. *Nano Lett.* **2011**, *11*, 1106.

(28) Utama, M. I. B.; Belarre, F. J.; Magen, C.; Peng, B.; Arbiol, J.; Xiong, Q. *Nano Lett.* **2012**, DOI: 10.1021/nl300554t.

(29) Utama, M. I. B.; Zhang, Q.; Jia, S.; Li, D.; Wang, J.; Xiong, Q. *ACS Nano* **2012**, *6*, 2281.

(30) Wyckoff, R. W. G. *Crystal Structures*; Krieger: Malabar, FL, 1986.

(31) Liu, Z.-H.; Brown, N. M. D.; McKinley, A. *Appl. Surf. Sci.* **1997**, *108*, 319.

(32) Li, Y.; Wang, G.; Zhu, X.; Liu, M.; Ye, C.; Chen, X.; Wang, Y. Y.; He, K.; Wang, L.; Ma, X. C.; Zhang, H.; Dai, X.; Fang, Z.; Xie, X.; Liu, Y.; Qi, X. L.; Jia, J. F.; Zhang, S. C.; Xue, Q. K. *Adv. Mater.* **2010**, *22*, 4002.